Article:

Wang, Q., Wang, X., Chen, H. et al. (4 more authors) (2019) An effective localization method for mixed far-field and near-field strictly non-circular sources. Digital Signal Processing, 94. pp. 125-136. ISSN 1051-2004

https://doi.org/10.1016/j.dsp.2019.06.003

An Effective Localization Method for Mixed Far-Field and Near-Field Strictly Non-circular Sources

Qing Wang[a], Xian Wang[a], Hua Chen[b,*], Xiaotian Zhu[a], Wei Liu[c], Weiqing Yan[d], Laihua Wang[e]

[a]*School of Electrical and Information Engineering, Tianjin University, Tianjin 300072, P. R. China.*
[b]*Faculty of Information Science and Engineering, Ningbo University, Ningbo 315211, P. R. China.*
[c]*Department of Electronic and Electrical Engineering, University of Sheffield, Sheffield S1 3JD, UK.*
[d]*School of Computer and Control Engineering, Yantai University, Yantai 264005, P. R. China.*
[e]*School of software Engineering, Qufu Normal University, Jining 273165, P. R. China*

Abstract

In this paper, an effective direction-of-arrival (DOA) and range estimations method for mixed far-field and near-field non-circular sources is proposed based on a large centrosymmetric uniform linear array (ULA). By exploiting the non-circularity of the sources, an extended signal is generated by concatenating the received array data and its conjugate counterparts. Then the DOAs of far-field signals are estimated based on the extended covariance matrix with the traditional MUSIC algorithm. After eliminating the far-field components from the extended signal subspace, the extended covariance matrix of the near-field signals is obtained. Thus a near-field estimator is constructed based on symmetric property of the extended array manifold where the generalized ESPRIT method is adopted to estimate the DOAs of near-field sources. Finally, the range estimator is derived using the DOA estimations of near-field sources. Simulation results are provided to validate that the proposed method has achieved a better performance than existing ones and is quite suitable for massive MIMO (multiple-input multiple-out) system.

---

[*] Corresponding author

Email addresses: `wangq@tju.edu.cn` (Qing Wang), `2213457603@qq.com` (Xian Wang), `dkchenhua0714@hotmail.com` (Hua Chen), `w.liu@sheffield.ac.uk` (Wei Liu)

Preprint submitted to Digital Signal Processing *June 20, 2019*

Keywords:
DOA estimation, far-field, near-field, non-circular signals, massive MIMO.

---

1. Introduction

The massive MIMO provides a new perspective for increasing the spectral efficiency and data rate to relieve the wireless mobile traffic, which is growing at an exponential pace, by making the use of a large excess of service antennas over active terminals and time-division duplex operation. Base stations (BSs) with 64 fully digital transceiver chains were commercially deployed in several countries, and the key ingredients of massive MIMO have made it into the 5G standard. In a word, massive MIMO became a reality for cellular networks [1].

In massive MIMO systems, each BS is equipped with a hundred or a few hundred antennas. With the extensive spatial freedoms offered by large antenna arrays, abundant users are expected to occupy the same set of time and frequency resources with negligible interference, thus circumventing the longstanding bandwidth limitation in wireless communications [2].

Attracted by the new characteristics of the massive MIMO technique, a lot of researchers have devoted to related exploration [3, 4]. Among these studies, one of hotspots is the mitigation or elimination of inter-cell interference caused by the non-orthogonality of pilot sequences of different cell users. To solve this issue, algorithm design [5], pilot design [6] and beamforming [7] are three typical strategies adopted by massive MIMO systems. However, for the first two strategies, they either suffer from higher computational complexity or offer middling performance, while the last one, assisted by DOA estimation has become an effective scheme. Accordingly, accurate DOA estimation becomes one of the significant research directions of massive MIMO system.

For the DOA estimation, various algorithms have been proposed to deal with the problem in the past decades, and most of them aim to locate either far-field signals [8–16] or near-field signals [17–20]. However, in some practical applications, far-field and near-field signals can be present at the same time.

Taking the active user localization in massive MIMO system for instance, the large antenna array exploited by the massive MIMO system contributes to a large Rayleigh distance, and this means that the far-field model which is a plane wave approximation over the array may be no longer suitable and the channel can not be seen as wide sense stationary [21]. The algorithms only designed for either far-field or near-field signals will become unreliable in this circumstance, so it is important to develop algorithms and methods to solve the localization problem with a mixture of near-field and far-field sources.

Some recent progress on the localization for the mixed far-field and near-field sources includes the work in [22], where a higher order statistic (HOS)-based algorithm is proposed, but its computational complexity is so high that limits its applications. To reduce the computational complexity, an efficient second-order statistics (SOS)-based method is presented in [23]. However, due to significant loss of the array aperture, its estimation accuracy is not high and the number of resolvable sources is also reduced. Based on the method in [23], Jiang proposed a simple and effective classification and localization method for mixed sources [24]. In [25], ESPRIT-like and polynomial rooting methods are developed to solve the problem with mixed sources, while in [26] Zuo. et al exploit the oblique projector to separate the mixed signals. In [27], Liu. et al first obtain the DOA and power information of far-field sources, and then locate the near-field sources based on the obtained information of far-field signals.

However, the aforementioned methods which solve the localization problem with mixed far-field and near-field signals do not consider the non-circularity of the impinging signals. In reality, non-circular signals are widely used in modern wireless communication systems, such as AM, BPSK modulated signals. The estimation performance can be improved if the non-circularity property of signals is exploited properly [28–30]. To the best of our knowledge, the estimation problem for mixed far-field and near-field non-circular sources has not been addressed yet, let alone based on the massive MIMO system.

In this paper, we aim to tackle the estimation problem for mixed non-circular sources by proposing an efficient localization method based on a large ULA.

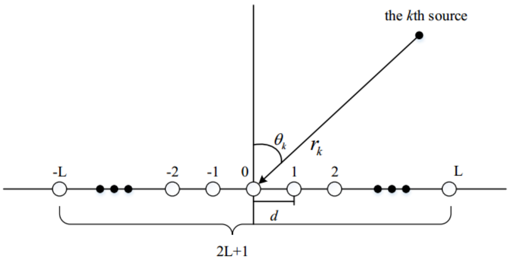

Fig. 1: Uniform linear array configuration.

Firstly, we combine the received array data and its conjugate counterpart to construct a new data vector, based on which the extended signal subspace and noise subspace are derived. Secondly, the extended covariance matrix and the DOA estimator of far-field sources are obtained from the extended signal subspace. Finally, the DOAs and the range parameters of near-field sources are obtained based on the symmetric property of the extended array manifold and the extended covariance matrix of near-field signals. Although the computational complexity of the proposed method is the highest due to the operations associated with the extended covariance matrix, the numerical simulations indicate its performance is the best among the existing ones.

Notations: $(\cdot)^*$, $(\cdot)^T$, $(\cdot)^H$, $(\cdot)^{-1}$ and $(\cdot)^\dagger$ represent conjugation, transpose, conjugate transpose, inverse and pseudo inverse, respectively; $E[\cdot]$ is the expectation operation; $diag(\cdot)$ stands for the diagonalization operation; $\mathbf{I}_\omega$ denotes the $\omega \times \omega$ identity matrix; $\det[\cdot]$ indicates the determinant of a matrix; $\|\cdot\|$ denotes the l_2 norm.

2. Problem formulation

In this paper, we assume that the number of impinging signals is known or estimated by some existing signal number detection techniques in advance [31]. Suppose there are M uncorrelated and non-circular narrowband signals (such as AM, BPSK modulated signals) impinging upon a large ULA of $K = 2L + 1$ sensors with M_1 near-field sources $s_{k_N}(t)(k_N = 1, 2, \ldots, M_1)$ and $M - M_1$ far-field sources $s_{k_F}(t)(k_F = M_1+1,\ldots,M)$, where t is the sample index, with $t = 1,2,\cdots,T$. The spacing between adjacent sensors is d (Fig. 1). Let the center element of array be reference point, then the received data vector at sample t can be expressed as

$$\mathbf{x}(t) = \mathbf{A}_N\mathbf{s}_N(t) + \mathbf{A}_F\mathbf{s}_F(t) + \mathbf{n}(t) \tag{1}$$

where $\mathbf{x}(t) = [x_{-L}(t),\cdots,x_{-1}(t),x_0(t),x_1(t),\cdots,x_L(t)]^T$, $\mathbf{A}_N= [\mathbf{a}_N(\theta_1,r_1),\cdots,$ $\mathbf{a}_N(\theta_{k_N},r_{k_N}),\cdots,\mathbf{a}_N(\theta_{M_1},r_{M_1})]$ and $\mathbf{s}_N(t)= [s_1(t),\cdots,s_{M_1}(t)]^T$ are the array steering matrix and the signal vectors of near-field signals, respectively. While $\mathbf{A}_F= [\mathbf{a}_F(\theta_{M_1+1}),\cdots,\mathbf{a}_F(\theta_{k_F}),\cdots,\mathbf{a}_F(\theta_M)]$ and $\mathbf{s}_F(t)= [s_{M_1+1}(t),\cdots,s_M(t)]^T$ are the array steering matrix and the signal vectors of far-field signals, respectively. And $\mathbf{n}(t)= [n_{-L}(t),\cdots,n_{-1}(t),n_0(t),n_1(t),\cdots,n_L(t)]^T$ represents circular additive white Gaussian noise with power σ^2, which is uncorrelated with the impinging signals.

The near-field steering vector $\mathbf{a}_N(\theta_{k_N},r_{k_N})$ and far-field steering vector $\mathbf{a}_F(\theta_{k_F})$ can be expressed in details as follow

$$\begin{aligned}\mathbf{a}_N(\theta_{k_N},r_{k_N}) = [&e^{j(-L\gamma_{k_N}+L^2\phi_{k_N})},\cdots,e^{j(-\gamma_{k_N}+\phi_{k_N})},1,\\ &e^{j(\gamma_{k_N}+\phi_{k_N})},\cdots,e^{j(L\gamma_{k_N}+L^2\phi_{k_N})}]^T\end{aligned} \tag{2}$$

$$\mathbf{a}_F(\theta_{k_F}) = [e^{j(-L\gamma_{k_F})},\cdots,e^{j(-\gamma_{k_F})},1,e^{j(\gamma_{k_F})},\cdots,e^{j(L\gamma_{k_F})}]^T \tag{3}$$

where $\gamma_{k_N} = -2\pi d sin\theta_{k_N}/\lambda$, $\phi_{k_N} = \pi d^2 cos^2\theta_{k_N}/(\lambda r_{k_N})$, $\gamma_{k_F} = -2\pi d sin\theta_{k_F}/\lambda$. λ is the wavelength, $\theta_k \in \left[-\frac{\pi}{2},\frac{\pi}{2}\right]$ $(k = 1,\cdots M)$ presents the DOA of the kth source, and r_{k_N} $(k_N = 1,\cdots M_1)$ denotes the range parameter of the k_Nth near-field source.

Due to the non-circularity of the sources, the signal vectors $\mathbf{s}_N(t)$ and $\mathbf{s}_F(t)$ can be expressed as

$$\mathbf{s}_N(t)=\boldsymbol{\psi}_N^{1/2}\mathbf{s}_{N_0}(\mathrm{t}) \tag{4}$$

$$\mathbf{s}_F(t)=\boldsymbol{\psi}_F^{1/2}\mathbf{s}_{F_0}(\mathrm{t}) \tag{5}$$

where $\mathbf{s}_{N_0}(t) = [s_{0,1}(t),\cdots,s_{0,M_1}(t)]^T$ is the zero-phase version of near-field signal $s_{k_N}(t)$, $k_N = 1,\cdots,M_1$, and $\mathbf{s}_{F_0} = [s_{o,M_1+1}(t),\cdots,s_{o,M}(t)]^T$ is the zero-phase version of far-field signal $s_{k_F}(t)$, $k_F = M_1+1, \cdots, M$. The diagonal matrices $\boldsymbol{\psi}_N^{1/2} = diag(e^{j\psi_1/2}, \cdots, e^{j\psi_{M_1}/2})$ and $\boldsymbol{\psi}_F^{1/2} = diag(e^{j\psi_{M_1+1}/2}, \cdots, e^{j\psi_M/2})$ have the arbitrary phase shifts of the near-field and far-field sources, respectively. And $\psi_k, k = 1, \cdots, M$ is the original phase of source signal $s_k(t), k = 1, \cdots, M$.

Thus, the conjugate counterpart of the received data vector $\mathbf{x}(t)$ can be written as

$$\begin{aligned}
\mathbf{x}^*(\mathrm{t}) = {} & [\mathbf{A}_N\mathbf{s}_N(\mathrm{t})+\mathbf{A}_F\mathbf{s}_F(\mathrm{t})+\mathbf{n}(\mathrm{t})]^* \\
& = \mathbf{A}_N^*\mathbf{s}_N^*(\mathrm{t})+\mathbf{A}_F^*\mathbf{s}_F^*(\mathrm{t})+\mathbf{n}^*(\mathrm{t}) \\
& = \mathbf{A}_N^*(\boldsymbol{\psi}_N^{1/2}\mathbf{s}_{N_0}(t))^* + \mathbf{A}_F^*(\boldsymbol{\psi}_F^{1/2}\mathbf{s}_{F_0}(t))^*+\mathbf{n}^*(\mathrm{t}) \\
& = \mathbf{A}_N^*\boldsymbol{\psi}_N^{-1/2}\mathbf{s}_{N_0}^*(t) + \mathbf{A}_F^*\boldsymbol{\psi}_F^{-1/2}\mathbf{s}_{F_0}^*(t)+\mathbf{n}^*(\mathrm{t}) \\
& = \mathbf{A}_N^*\boldsymbol{\psi}_N^{-1}\mathbf{s}_N(t) + \mathbf{A}_F^*\boldsymbol{\psi}_F^{-1}\mathbf{s}_F(t)+\mathbf{n}^*(\mathrm{t}) \\
& = \mathbf{A}_N^*\boldsymbol{\psi}_N^*\mathbf{s}_N(t) + \mathbf{A}_F^*\boldsymbol{\psi}_F^*\mathbf{s}_F(t)+\mathbf{n}^*(\mathrm{t})
\end{aligned} \tag{6}$$

3. The proposed method

3.1. Estimator of far-field sources

First, we define a new vector $\mathbf{Y}(t)$ by combining the observed data vector $\mathbf{x}(t)$ and its conjugate counterpart $\mathbf{x}^*(t)$ as follows

$$\begin{aligned}
\mathbf{Y}(t) &= \begin{bmatrix} \mathbf{x}(t) \\ \mathbf{x}^*(t) \end{bmatrix} \\
&= \begin{bmatrix} \mathbf{A}_N \\ \mathbf{A}_N^*\boldsymbol{\psi}_N^* \end{bmatrix} \mathbf{s}_N(t) + \begin{bmatrix} \mathbf{A}_F \\ \mathbf{A}_F^*\boldsymbol{\psi}_F^* \end{bmatrix} \mathbf{s}_F(t) + \begin{bmatrix} \mathbf{n}(t) \\ \mathbf{n}^*(t) \end{bmatrix} \\
&= \mathbf{A}_{eN}\mathbf{s}_N(t) + \mathbf{A}_{eF}\mathbf{s}_F(t) + \mathbf{n}_e(t)
\end{aligned} \tag{7}$$

where $\mathbf{A}_{eN} = \begin{bmatrix} \mathbf{A}_N \\ \mathbf{A}_N^*\boldsymbol{\psi}_N^* \end{bmatrix} = [\tilde{\mathbf{a}}_N(\theta_1, r_1, \psi_1), \cdots, \tilde{\mathbf{a}}_N(\theta_{M_1}, r_{M_1}, \psi_{M_1})]$, and $\tilde{\mathbf{a}}_N(\theta_{k_N}, r_{k_N}, \psi_{k_N}) = \begin{bmatrix} \mathbf{a}_N(\theta_{k_N}, r_{k_N}) \\ \mathbf{a}_N{}^*(\theta_{k_N}, r_{k_N})e^{-j\psi_{k_N}} \end{bmatrix}$, $k_N = 1, \cdots, M_1$; $\mathbf{A}_{eF} = \begin{bmatrix} \mathbf{A}_F \\ \mathbf{A}_F^*\boldsymbol{\psi}_F^* \end{bmatrix} = [\tilde{\mathbf{a}}_F(\theta_{M_1+1}, \psi_{M_1+1}), \cdots, \tilde{\mathbf{a}}_F(\theta_M, \psi_M)]$, and $\tilde{\mathbf{a}}_F(\theta_{k_F}, \psi_{k_F}) = \begin{bmatrix} \mathbf{a}_F(\theta_{k_F}) \\ \mathbf{a}_F{}^*(\theta_{k_F})e^{-j\psi_{k_F}} \end{bmatrix}$, $k_F = M_1 + 1, \cdots, M$.

Then the covariance matrix of $\mathbf{Y}(t)$ is calculated by

$$\begin{aligned}\mathbf{R} &= E[\mathbf{Y}(t)\mathbf{Y}^H(t)] \\ &= \mathbf{A}_{eN}\mathbf{R}_{sN}\mathbf{A}_{eN}{}^H + \mathbf{A}_{eF}\mathbf{R}_{sF}\mathbf{A}_{eF}{}^H + \sigma^2\mathbf{I}_{2K} \\ &= \mathbf{R}_N + \mathbf{R}_F + \sigma^2\mathbf{I}_{2K}\end{aligned} \tag{8}$$

where $\mathbf{R}_N$ is the near-field covariance matrix of the received data, and $\mathbf{R}_{sN} = E[\mathbf{s}_N(t)\mathbf{s}_N{}^H(t)]$ is the covariance matrix of near-field source signals. $\mathbf{R}_F$ is the far-field covariance matrix of the received data, and $\mathbf{R}_{sF} = E[\mathbf{s}_F(t)\mathbf{s}_F{}^H(t)]$ represent the corresponding far-field ones.

The eigenvalue decomposition of $\mathbf{R}$ is given by

$$\mathbf{R} = \mathbf{U_s\Lambda_s U_s}^{\mathbf{H}} + \mathbf{U_n\Lambda_n U_n}^{\mathbf{H}} = \mathbf{U\Lambda U^H} \tag{9}$$

where the $2K \times M$ matrix $\mathbf{U}_s$ and the $2K \times (2K - M)$ matrix $\mathbf{U}_n$ are the signal subspace and noise subspace, respectively. The $M \times M$ matrix $\mathbf{\Lambda}_s = diag(\lambda_1, \lambda_2, \ldots, \lambda_M)$ and the $(2K-M)\times(2K-M)$ matrix $\mathbf{\Lambda}_n = diag(\lambda_{M+1}, \lambda_{M+2}, \ldots, \lambda_{2K})$ are diagonal matrices; $\mathbf{\Lambda} = diag(\lambda_1, \lambda_2, \ldots, \lambda_{2K})$, where $\lambda_1 \geq \lambda_2 \geq \cdots \geq \lambda_M > \lambda_{M+1} = \cdots = \lambda_{2K} = \sigma^2$ are the eigenvalues of $\mathbf{R}$.

Based on the orthogonality between $\mathbf{U}_n$ and $\tilde{\mathbf{a}}_F(\theta_{k_F}, \psi_{k_F})$, the following result can be obtained

$$\begin{aligned}\mathbf{U_n}^H\tilde{\mathbf{a}}_F(\theta_{k_F}, \psi_{k_F}) &= \mathbf{U_n}^H\begin{bmatrix}\mathbf{a_F}(\theta_{k_F}) \\ \mathbf{a_F}^*(\theta_{k_F})e^{-j\psi_{k_F}}\end{bmatrix} \\ = \mathbf{U_n}^H\begin{bmatrix}\mathbf{a_F}(\theta_{k_F}) & \\ & \mathbf{a_F}^*(\theta_{k_F})\end{bmatrix}&\begin{bmatrix}1 \\ e^{-j\psi_{k_F}}\end{bmatrix} = \mathbf{0}\end{aligned} \tag{10}$$

Based on the rank reduction (RARE) principle [32], according to (10), $\mathbf{U_n}^H\begin{bmatrix}\mathbf{a_F}(\theta_{k_F}) & \\ & \mathbf{a_F}^*(\theta_{k_F})\end{bmatrix} = \mathbf{0}$ for $\begin{bmatrix}1 \\ e^{-j\psi_{k_F}}\end{bmatrix} \neq \mathbf{0}$. Define a $2K \times 2$ matrix $\mathbf{V}_F(\theta) = \begin{bmatrix}\mathbf{a}_F(\theta) & \\ & \mathbf{a}_F{}^*(\theta)\end{bmatrix}$, which is only related to θ, and a 2×2 matrix $\mathbf{Q}_F(\theta) = \mathbf{V}_F(\theta)^H\mathbf{U}_n\mathbf{U}_n{}^H\mathbf{V}_F(\theta)$. If θ is not the true DOA angle of far-field sources, $\mathbf{Q}_F(\theta)$ will be of full rank, which means (10) holds true only when θ is the true DOA angle of the far-field signals ($\mathbf{Q}_F(\theta)$ drops rank). Since the covariance matrix of $\mathbf{Y}(t)$ is obtained from a finite number of samples, the reduction of the rank of $\mathbf{Q}_F(\theta)$ can roughly be replaced by the minimum of the determinant of $\mathbf{Q}_F(\theta)$. Therefore, we can get the estimator of θ for far-field sources as follows

$$f_F(\theta) = \frac{1}{\det\{\mathbf{Q}_F(\theta)\}} = \frac{1}{\det\{\mathbf{V}_F(\theta)^H \mathbf{U}_n {\mathbf{U}_n}^H \mathbf{V}_F(\theta)\}} \tag{11}$$

By searching over the range of $\theta \in \left[-\frac{\pi}{2}, \frac{\pi}{2}\right]$, the DOAs of far-field sources can be obtained from the peaks of $f_F(\theta)$.

3.2. Estimator of near-field sources

Since $\mathbf{U}_n$ is orthogonal to $\tilde{\mathbf{a}}_N(\theta_{k_N}, r_{k_N}, \psi_{k_N})$, the following equation can be obtained

$$\begin{aligned} {\mathbf{U}_n}^H \tilde{\mathbf{a}}_N(\theta_{k_N}, r_{k_N}, \psi_{k_N}) &= {\mathbf{U}_n}^H \begin{bmatrix} \mathbf{a}_N(\theta_{k_N}, r_{k_N}) \\ {\mathbf{a}_N}^*(\theta_{k_N}, r_{k_N}) e^{-j\psi_{k_N}} \end{bmatrix} \\ = {\mathbf{U}_n}^H \begin{bmatrix} \mathbf{a}_N(\theta_{k_N}, r_{k_N}) & \\ & {\mathbf{a}_N}^*(\theta_{k_N}, r_{k_N}) \end{bmatrix} &\begin{bmatrix} 1 \\ e^{-j\psi_{k_N}} \end{bmatrix} = \mathbf{0} \end{aligned} \tag{12}$$

Again based on the RARE principle, we get the estimator of near-field sources as follows

$$f_N(\theta, r) = \frac{1}{\det\{\mathbf{P}_N(\theta, r)\}} = \frac{1}{\det\{\mathbf{V}_N(\theta, r)^H \mathbf{U}_n {\mathbf{U}_n}^H \mathbf{V}_N(\theta, r)\}} \tag{13}$$

where $\mathbf{V}_N(\theta, r) = \begin{bmatrix} \mathbf{a}_N(\theta, r) & \\ & {\mathbf{a}_N}^*(\theta, r) \end{bmatrix}$, $\mathbf{P}_N(\theta, r) = \mathbf{V}_N(\theta, r)^H \mathbf{U}_n {\mathbf{U}_n}^H \mathbf{V}_N(\theta, r)$.

It's obvious that $f_N(\theta, r)$ has two parameters (include θ and r) to be estimated, in other words, formulation (13) is a two-dimensional search problem. To avoid the complexity, we adopt a new strategy to estimate these two parameters: 1) Estimate the DOA of the near-field sources firstly. 2) Estimate the range r based on formulation (13) after the DOA have been estimated in the former step.

3.2.1. The derivation of the covariance matrix for near-field sources

To estimate the DOA of near-field sources, we first estimate the far-field covariance matrix from the obtained DOA and power information of far-field signals, and then derive the near-field covariance matrix, based on which an DOA estimator for near-field sources can be developed.

Based on (8) and (9), we have

$$\begin{aligned}
&\mathbf{U^H}\mathbf{R}\mathbf{U} = \mathbf{U^H}\mathbf{U}\boldsymbol{\Lambda}\mathbf{U^H}\mathbf{U} = \boldsymbol{\Lambda}\\
&=\mathbf{U^H}(\mathbf{A}_{eN}\mathbf{R}_{sN}{\mathbf{A}_{eN}}^H + \mathbf{A}_{eF}\mathbf{R}_{sF}{\mathbf{A}_{eF}}^H + \sigma^2\mathbf{I}_{2K})\mathbf{U}\\
&=\mathbf{U^H}(\mathbf{A}_{eN}\mathbf{R}_{sN}{\mathbf{A}_{eN}}^H + \mathbf{A}_{eF}\mathbf{R}_{sF}{\mathbf{A}_{eF}}^H)\mathbf{U} + \sigma^2\mathbf{U^H}\mathbf{U}\\
&=\mathbf{U^H}(\mathbf{A}_e\mathbf{R}_s{\mathbf{A}_e}^H)\mathbf{U} + \sigma^2\mathbf{I}_{2K}
\end{aligned} \tag{14}$$

where $\mathbf{A}_e\mathbf{R}_s{\mathbf{A}_e}^H = \mathbf{A}_{eN}\mathbf{R}_{sN}{\mathbf{A}_{eN}}^H + \mathbf{A}_{eF}\mathbf{R}_{sF}{\mathbf{A}_{eF}}^H$, thus

$$\mathbf{U^H}(\mathbf{A}_e\mathbf{R}_s{\mathbf{A}_e}^H)\mathbf{U} = \boldsymbol{\Lambda} - \sigma^2\mathbf{I}_{2K} \tag{15}$$

$$= diag(\alpha_1, \alpha_2, \cdots, \alpha_M, 0, \cdots, 0) \tag{16}$$

where $\alpha_1, \alpha_2, \cdots, \alpha_M$ are the eigenvalues of the covariance matrix of $\tilde{\mathbf{Y}}(t)$, and

$$\tilde{\mathbf{Y}}(t) = \begin{bmatrix} \tilde{\mathbf{x}}(t) \\ \tilde{\mathbf{x}}^*(t) \end{bmatrix} \tag{17}$$

where

$$\tilde{\mathbf{x}}(t) = \mathbf{A}_N\mathbf{s}_N(t) + \mathbf{A}_F\mathbf{s}_F(t) \tag{18}$$

It is obvious that $\tilde{\mathbf{x}}(t)$ doesn't include additive noise $\mathbf{n}(t)$ compared with $\mathbf{x}(t)$. Then we obtain

$$\mathbf{U}_s(\boldsymbol{\Lambda}_s - \sigma^2\mathbf{I}_M)\mathbf{U}_s^H = \mathbf{A}_e\mathbf{R}_s\mathbf{A}_e^H \tag{19}$$

where the noise power σ^2 can be obtained by averaging the $2K - M$ smallest eigenvalues of $\mathbf{R}$.

We can calculate the power of the k_Fth far-field source as follows

$$
\begin{aligned}
\sigma_{k_F}^2 &= \left\{\mathbf{e}_{k_F}^H diag\{1/\sigma_1^2, \cdots, 1/\sigma_M^2\}\mathbf{e}_{k_F}\right\}^{-1} \\
&= \left\{\left[\mathbf{A}_e^{\dagger}\tilde{\mathbf{a}}_F(\theta_{k_F}, \psi_{k_F})\right]^H \mathbf{R}_s^{\dagger} \left[\mathbf{A}_e^{\dagger}\tilde{\mathbf{a}}_F(\theta_{k_F}, \psi_{k_F})\right]\right\}^{-1} \\
&= \left\{\tilde{\mathbf{a}}_F^H(\theta_{k_F}, \psi_{k_F}) \left[\mathbf{U}_s(\mathbf{\Lambda}_s - \sigma^2\mathbf{I}_M){\mathbf{U}_s}^H\right]^{\dagger} \tilde{\mathbf{a}}_F(\theta_{k_F}, \psi_{k_F})\right\}^{-1} \\
&= \left\{\begin{bmatrix} 1 \\ e^{-j\psi_{k_F}} \end{bmatrix}^H \begin{bmatrix} \mathbf{a}_F(\theta_{k_F}) & \\ & {\mathbf{a}_F}^*(\theta_{k_F}) \end{bmatrix}^H \cdot \right. \\
&\qquad \left[\mathbf{U}_s(\mathbf{\Lambda}_s - \sigma^2\mathbf{I}_M){\mathbf{U}_s}^H\right]^{\dagger} \cdot \\
&\qquad \left. \begin{bmatrix} \mathbf{a}_F(\theta_{k_F}) & \\ & {\mathbf{a}_F}^*(\theta_{k_F}) \end{bmatrix} \begin{bmatrix} 1 \\ e^{-j\psi_{k_F}} \end{bmatrix}\right\}^{-1}
\end{aligned} \tag{20}
$$

where $\mathbf{e}_{k_F}$ is the k_Fth column vector of the identity matrix $\mathbf{I}_M$.

To calculate the phase shifts ψ_{k_F} of far-field sources, we adopt a general method in [20, 33]. Partitioning $\mathbf{U}_n$ into $\mathbf{U}_n = \begin{bmatrix} \mathbf{U}_{n1} \\ \mathbf{U}_{n2} \end{bmatrix}$, where $\mathbf{U}_{n1}$ and $\mathbf{U}_{n2}$ are two submatrices of the same size $K \times (2K - M)$. We obtain

$$
\begin{aligned}
& g(\theta_{k_F}, \psi_{k_F}) = \widetilde{\mathbf{a}}_F^H(\theta_{k_F}, \psi_{k_F})\mathbf{U}_n\mathbf{U}_n^H\widetilde{\mathbf{a}}_F(\theta_{k_F}, \psi_{k_F}) \\
& = \widetilde{\mathbf{a}}_F^H(\theta_{k_F}, \psi_{k_F}) \begin{bmatrix} \mathbf{U}_{n1}\mathbf{U}_{n1}^H & \mathbf{U}_{n1}\mathbf{U}_{n2}^H \\ \mathbf{U}_{n2}\mathbf{U}_{n1}^H & \mathbf{U}_{n2}\mathbf{U}_{n2}^H \end{bmatrix} \widetilde{\mathbf{a}}_F(\theta_{k_F}, \psi_{k_F}) \\
& = \begin{bmatrix} \mathbf{a}_F(\theta_{k_F}) \\ {\mathbf{a}_F}^*(\theta_{k_F})e^{-j\psi_{k_F}} \end{bmatrix}^H \begin{bmatrix} \mathbf{U}_{n1}\mathbf{U}_{n1}^H & \mathbf{U}_{n1}\mathbf{U}_{n2}^H \\ \mathbf{U}_{n2}\mathbf{U}_{n1}^H & \mathbf{U}_{n2}\mathbf{U}_{n2}^H \end{bmatrix} \begin{bmatrix} \mathbf{a}_F(\theta_{k_F}) \\ {\mathbf{a}_F}^*(\theta_{k_F})e^{-j\psi_{k_F}} \end{bmatrix} \\
& = \begin{bmatrix} 1 \\ e^{-j\psi_{k_F}} \end{bmatrix}^H \begin{bmatrix} \mathbf{a}_F(\theta_{k_F}) & \\ & {\mathbf{a}_F}^*(\theta_{k_F}) \end{bmatrix}^H \begin{bmatrix} \mathbf{U}_{n1}\mathbf{U}_{n1}^H & \mathbf{U}_{n1}\mathbf{U}_{n2}^H \\ \mathbf{U}_{n2}\mathbf{U}_{n1}^H & \mathbf{U}_{n2}\mathbf{U}_{n2}^H \end{bmatrix} \\
& \quad \begin{bmatrix} \mathbf{a}_F(\theta_{k_F}) & \\ & {\mathbf{a}_F}^*(\theta_{k_F}) \end{bmatrix} \begin{bmatrix} 1 \\ e^{-j\psi_{k_F}} \end{bmatrix} \\
& = \begin{bmatrix} 1 \\ e^{-j\psi_{k_F}} \end{bmatrix}^H \begin{bmatrix} \mathbf{a}_F^H(\theta_{k_F})\mathbf{U}_{n1}\mathbf{U}_{n1}^H\mathbf{a}_F(\theta_{k_F}) & \mathbf{a}_F^H(\theta_{k_F})\mathbf{U}_{n1}\mathbf{U}_{n2}^H{\mathbf{a}_F}^*(\theta_{k_F}) \\ (\mathbf{a}_F^H(\theta_{k_F})\mathbf{U}_{n1}\mathbf{U}_{n2}^H{\mathbf{a}_F}^*(\theta_{k_F}))^H & \mathbf{a}_F^T(\theta_{k_F})\mathbf{U}_{n2}\mathbf{U}_{n2}^H{\mathbf{a}_F}^*(\theta_{k_F}) \end{bmatrix} \\
& \quad \begin{bmatrix} 1 \\ e^{-j\psi_{k_F}} \end{bmatrix} \\
& = \mathbf{q}(\psi_{k_F})^H\mathbf{C}(\theta_{k_F})\mathbf{q}(\psi_{k_F})
\end{aligned} \tag{21}
$$

where $\mathbf{C}(\theta_{k_F}) = \begin{bmatrix} \mathbf{a}_F^H(\theta_{k_F})\mathbf{U}_{n1}\mathbf{U}_{n1}^H\mathbf{a}_F(\theta_{k_F}) & \mathbf{a}_F^H(\theta_{k_F})\mathbf{U}_{n1}\mathbf{U}_{n2}^H\mathbf{a}_F^*(\theta_{k_F}) \\ (\mathbf{a}_F^H(\theta_{k_F})\mathbf{U}_{n1}\mathbf{U}_{n2}^H\mathbf{a}_F^*(\theta_{k_F}))^H & \mathbf{a}_F^T(\theta_{k_F})\mathbf{U}_{n2}\mathbf{U}_{n2}^H\mathbf{a}_F^*(\theta_{k_F}) \end{bmatrix}$ and $\mathbf{q}(\psi_{k_F}) = [1, e^{-j\psi_{k_F}}]^T$.

Setting the partial derivative of $g(\theta_{k_F}, \psi_{k_F})$ with respect to ψ_{k_F} to zero, i.e.,$\partial g(\theta_{k_F}, \psi_{k_F})/\partial\psi_{k_F} = 0$, we have

$$e^{j\psi_{k_F}} = \pm \frac{\mathbf{a}_F^H(\theta_{k_F})\mathbf{U}_{n1}\mathbf{U}_{n2}^H\mathbf{a}_F^*(\theta_{k_F})}{\left\|\mathbf{a}_F^H(\theta_{k_F})\mathbf{U}_{n1}\mathbf{U}_{n2}^H\mathbf{a}_F^*(\theta_{k_F})\right\|} \tag{22}$$

The minima of (21) are obtained when the sign of the right-hand side of (22) is minus. Therefore, we can get the ultimate expression for $e^{j\psi_{k_F}}$.

Substituting the estimated $\hat{\theta}_{k_F}$ into (20), we then obtain the power of the far-field signals. Then the far-field covariance matrix can be derived as follows

$$\mathbf{R}_F = \mathbf{A}_{eF} diag(\sigma_{M_1+1}^2, \sigma_{M_1+2}^2, \cdots, \sigma_M^2)\mathbf{A}_{eF}^H \tag{23}$$

and the near-field covariance matrix is then given by

$$\mathbf{R}_N = \mathbf{U}_s(\mathbf{\Lambda}_s - \sigma^2\mathbf{I}_M){\mathbf{U}_s}^H - \mathbf{R}_F \tag{24}$$

Apply eigenvalue decomposition to $\mathbf{R}_N$, leading to

$$\mathbf{R}_N = \mathbf{E}_s\mathbf{\Delta}_s\mathbf{E}_s^H + \mathbf{E}_n\mathbf{\Delta}_n\mathbf{E}_n^H \tag{25}$$

where the $2K \times M_1$ matrix $\mathbf{E}_s$ and the $2K \times (2K - M_1)$ matrix $\mathbf{E}_n$ are the signal subspace and noise subspace, respectively. The diagonal matrix $\mathbf{\Delta}_s$ includes the M_1 largest eigenvalues and $\mathbf{\Delta}_n$ has the $2K - M_1$ smallest ones.

3.2.2. DOA estimation for near-field sources

With the covariance matrix of near-field sources being obtained, in other words, the information of near-field sources is separated from the mixed sources, we further study the derivation of DOA estimator for near-field sources.

By analysing the centrosymmetric structure of the ULA and exploring the inner relationship of the steering vectors, we find

$$\mathbf{J}_2\mathbf{a}_N(\theta_{k_N}, r_{k_N}){=}\mathbf{D}(\theta_{k_N})\mathbf{J}_1\mathbf{a}_N(\theta_{k_N}, r_{k_N}) \tag{26}$$

where $\mathbf{J}_1 = \begin{bmatrix} 0 & \cdots & 1 \\ \vdots & \ddots & \vdots \\ 1 & \cdots & 0 \end{bmatrix} \in K \times K$, $\mathbf{J}_2 = \begin{bmatrix} 1 & \cdots & 0 \\ \vdots & \ddots & \vdots \\ 0 & \cdots & 1 \end{bmatrix} \in K \times K$, $\mathbf{J}_1^{nc} = \begin{bmatrix} \mathbf{J}_1 & \mathbf{0} \\ \mathbf{0} & \mathbf{J}_1 \end{bmatrix}$, $\mathbf{J}_2^{nc} = \begin{bmatrix} \mathbf{J}_2 & \mathbf{0} \\ \mathbf{0} & \mathbf{J}_2 \end{bmatrix}$, and $\mathbf{D}(\theta_{k_N}) = diag\{e^{j(-2L\gamma_{k_N})}, \cdots, e^{j(-2\gamma_{k_N})}, 1, e^{j(2\gamma_{k_N})}, \cdots, e^{j(2L\gamma_{k_N})}\}$.

In fact, the formulation (26) is coincident with the key ingredient of the generalized ESPRIT (GESPRIT) algorithm [10]. For the GESPRIT algorithm, the inner relationship of the steering vectors is explored and each steering vector is reformulated as the product of itself and a diagonal matrix with some trivial transformation (in (26), the steering vector is $\mathbf{a}_N(\theta_{k_N}, r_{k_N})$ and the diagonal matrix is $\mathbf{D}(\theta_{k_N})$). While in the conventional ESPRIT algorithm, the relationship of the steering vectors is integrated and is shown as the relationship of the whole manifold [34]. Owing to the representation in (26), the DOAs to be estimated forms a mapping relationship to the corresponding steering vectors and thus can be evaluated one by one in the following analyses. Besides, this improvement makes the GESPRIT applicable to a much more general class array of geometries than assumed by the conventional ESPRIT algorithm.

Note that $\mathbf{J}_2\mathbf{a}_N^*(\theta_{k_N}, r_{k_N}) = \mathbf{D}^*(\theta_{k_N})\mathbf{J}_1\mathbf{a}_N^*(\theta_{k_N}, r_{k_N})$ by conjugating (26), therefore,

$$\begin{aligned}
&\mathbf{J}_2^{nc}\tilde{\mathbf{a}}_N(\theta_{k_N}, r_{k_N}, \psi_{k_N}) = \begin{bmatrix} \mathbf{J}_2\mathbf{a}_\mathrm{N}(\theta_{k_N}, r_{k_N}) \\ \mathbf{J}_2\mathbf{a}_N^*(\theta_{k_N}, r_{k_N})e^{-j\psi_{k_N}} \end{bmatrix} \\
&= \begin{bmatrix} \mathbf{D}(\theta_{k_N})\mathbf{J}_1\mathbf{a}_\mathrm{N}(\theta_{k_N}, r_{k_N}) \\ \mathbf{D}^*(\theta_{k_N})\mathbf{J}_1\mathbf{a}_N^*(\theta_{k_N}, r_{k_N})e^{-j\psi_{k_N}} \end{bmatrix} \\
&= \begin{bmatrix} \mathbf{D}(\theta_{k_N}) & 0 \\ 0 & \mathbf{D}^*(\theta_{k_N}) \end{bmatrix} \begin{bmatrix} \mathbf{J}_1 & 0 \\ 0 & \mathbf{J}_1 \end{bmatrix} \begin{bmatrix} \mathbf{a}_\mathrm{N}(\theta_{k_N}, r_{k_N}) \\ \mathbf{a}_N^*(\theta_{k_N}, r_{k_N})e^{-j\psi_{k_N}} \end{bmatrix} \\
&= \tilde{\mathbf{D}}(\theta_{k_N})\mathbf{J}_1^{nc}\tilde{\mathbf{a}}_N(\theta_{k_N}, r_{k_N}, \psi_{k_N})
\end{aligned} \tag{27}$$

where $\tilde{\mathbf{D}}(\theta_{k_N}) = \begin{bmatrix} \mathbf{D}(\theta_{\mathrm{k_N}}) & 0 \\ 0 & \mathbf{D}^*(\theta_{\mathrm{k_N}}) \end{bmatrix}$, so we get

$$\begin{aligned}
\mathbf{J}_2^{nc}\mathbf{A}_{eN} = [&\tilde{\mathbf{D}}(\theta_1)\mathbf{J}_1^{nc}\tilde{\mathbf{a}}_N(\theta_1, r_1, \psi_1), \cdots, \\
&\tilde{\mathbf{D}}(\theta_{k_N})\mathbf{J}_1^{nc}\tilde{\mathbf{a}}_N(\theta_{k_N}, r_{k_N}, \psi_{k_N}), \cdots, \\
&\tilde{\mathbf{D}}(\theta_K)\mathbf{J}_1^{nc}\tilde{\mathbf{a}}_N(\theta_{M_1}, r_{M_1}, \psi_{M_1})]
\end{aligned} \tag{28}$$

According to [20], there exists a full-rank $\mathrm{M}_1 \times \mathrm{M}_1$ matrix $\mathbf{G}$ satisfying $\mathbf{E}_s = \mathbf{A}_{\mathrm{eN}}\mathbf{G}$. And we can form a $2K \times 2K$ diagonal matrix:

$$\begin{aligned}\mathbf{\Phi}(\theta)=diag\{&e^{j(-2L\gamma)},\cdots,e^{j(-2\gamma)},1,e^{j(2\gamma)},\cdots,e^{j(2L\gamma)},\\&e^{j(2L\gamma)},\cdots,e^{j(2\gamma)},1,e^{j(-2\gamma)},\cdots,e^{j(-2L\gamma)}\}\end{aligned} \tag{29}$$

with $\gamma = -2\pi d \sin\theta/\lambda$.

Now we can construct the $2K \times M_1$ matrix:

$$\begin{aligned}\mathbf{Q}_N(\theta) &= \mathbf{J}_2^{nc}\mathbf{E}_s - \mathbf{\Phi}(\theta)\mathbf{J}_1^{nc}\mathbf{E}_s\\&= [(\tilde{\mathbf{D}}(\theta_1) - \mathbf{\Phi}(\theta))\mathbf{J}_1^{nc}\tilde{\mathbf{a}}_N(\theta_1, r_1, \psi_1), \cdots,\\&\quad (\tilde{\mathbf{D}}(\theta_{k_N}) - \mathbf{\Phi}(\theta))\mathbf{J}_1^{nc}\tilde{\mathbf{a}}_N(\theta_{k_N}, r_{k_N}, \psi_{k_N}), \cdots,\\&\quad (\tilde{\mathbf{D}}(\theta_{M1}) - \mathbf{\Phi}(\theta))\mathbf{J}_1^{nc}\tilde{\mathbf{a}}_N(\theta_{M_1}, r_{M_1}, \psi_{M_1})]\mathbf{G}\end{aligned} \tag{30}$$

For formulation (30), if θ is the true angle of the near-field sources, such as $\theta = \theta_{k_N}$, $k_N = 1, \cdots, M_1$, the k_Nth column of $\mathbf{Q}_N(\theta)$ will become zero, which means that the $M_1 \times M_1$ matrix $\mathbf{W}^H\mathbf{Q}_N(\theta)$ is singular, with $\mathbf{W}$ being an arbitrary $2K \times M_1$ full-rank matrix. A related discussion on the choice of $\mathbf{W}$ can be found in [35] from the traditional ESPRIT viewpoint. Therefore, we can have the estimator of θ for near-field sources as follows

$$f_N(\theta) = \frac{1}{\det\{\mathbf{W}^H\mathbf{Q}_N(\theta)\}} \tag{31}$$

where the range parameter r makes no difference to the estimation of the DOAs and for $\theta \in \left[-\frac{\pi}{2}, \frac{\pi}{2}\right]$, the DOAs of near-field sources can be obtained by finding the peaks of $f_N(\theta)$.

3.2.3. Range estimation of near-Field sources

By substituting the estimated $\hat{\theta}_{k_N}$ of near-field sources ($k_N = 1, 2, \cdots, M_1$) into (13), we can obtain the estimator of the range of near-field sources.

$$f_N(\hat{\theta}, r) = \frac{1}{\det\{\mathbf{P}_N(\hat{\theta}, r)\}} = \frac{1}{\det\{\mathbf{V}_N(\hat{\theta}, r)^H\mathbf{U}_n\mathbf{U}_n{}^H\mathbf{V}_N(\hat{\theta}, r)\}} \tag{32}$$

By searching within the range $r \in \left[0.62(D^3/\lambda)^{1/2}, 2D^2/\lambda\right]$, where D is the array aperture, the range of near-field signals can be obtained from the peaks of $f_N(\hat{\theta}, r)$. Note that the DOA and range estimates of near-field sources can be automatically paired without any additional operation.

3.3. Summary of the proposed method

The proposed method can be described as follows

```
Algorithm 1 The Proposed Method
    Step 1: Concatenate the original received vector $\mathbf{x}(t)$ and its conjugate counterpart $\mathbf{x}^*(t)$ to obtain the augment vector $\mathbf{Y}(t) = \begin{bmatrix} \mathbf{x}(t) \\ \mathbf{x}^*(t) \end{bmatrix}$.
    Step 2: Calculate the covariance matrix $\hat{\mathbf{R}}=\frac{1}{T}\sum_{t=1}^{T} Y(t)Y^H(t)$.
    Step 3: Implement the eigenvalue decomposition on $\hat{\mathbf{R}}$ to obtain the augment signal subspace $\hat{\mathbf{U}}_{\mathrm{s}}$ and augment noise subpace $\hat{\mathbf{U}}_{\mathrm{n}}$.
    Step 4: Similarly to the traditional MUSIC algorithm, obtain the DOAs $(\hat{\theta}_{k_F}, k_F = M_1 + 1, \cdots, M)$ of the far-field sources based on formulation (11).
    Step 5: Calculate noise power $(\hat{\sigma}^2_{k_F}, k_F = M_1 + 1, \cdots, M)$ of far-field signal space based on formulation (20).
    Step 6: Obtain the augment near-field signals covariance matrix $\hat{\mathbf{R}}_N$ based on formulation (24) after getting the augment far-field signals covariance matrix $\hat{\mathbf{R}}_F$ from formulation (23).
    Step 7: Implement the eigenvalue decomposition of $\hat{\mathbf{R}}_N$ to obtain the near-field signal subspace $\mathbf{E}_s$ and noise subspace $\mathbf{E}_n$.
    Step 8: Based on the generalized ESPRIT method, obtain the DOAs $(\hat{\theta}_{k_N}, k_N = 1, \cdots, M_1)$ of the near-field sources according to formulation (31).
    Step 9: Obtain the range $(\hat{r}_{k_N}, k_N = 1, \cdots, M_1)$ of the near-field source based on formulation (32) with $\hat{\theta}_{k_N}$ estimated in Step 8.
```

3.4. Discussion

3.4.1. Computational complexity

For the computational complexity of the proposed method, we compare it with He's method in [23], Zuo's method in [26], and Liu's method in [27]. The complexity lies mainly in constructing the covariance matrix and performing the eigendecomposition. For the method in [23], it is about $O((2L+1)^2\eta + (L+2)^2L + (2L+1)^3 + (L+2)^3)$; for Zuo's method, we have $O((2L+1)^2\eta +$

$(2L+1-M)^3+(2L+1)^3+(2L+1)^3)$; Liu's method in [27] has a complexity of $O((2L+1)^2\eta+(2L+1)^3+2(2L+1)^2+(2L+1)^3)$, while the proposed algorithm is $O((4L+2)^2\eta+(4L+2)^3+2(4L+2)^2+(4L+2)^3)$. We can see that the computational complexity of the proposed method is the highest due to the operations associated with the extended covariance matrix, but its performance is the best as the following simulation results will prove.

3.4.2. Array aperture

Since the augment vector $\mathbf{Y}(t)$ in the proposed method has higher dimension than the original received data $\mathbf{x}(t)$, the method actually extends the array aperture. Therefore, the proposed method can estimate more sources than other methods and it can estimate $2L$ sources at most with a ULA consisting of $2L+1$ elements. To verify it, a set of experiments is demonstrated in the fourth subsection of Section 4 to examine the largest number of the sources that can be detected by the proposed method for a given ULA.

3.4.3. Suitability for massive MIMO systems

The proposed method can be applied to the massive MIMO system. To prove this point, simulation verification is carried out in the last part of the simulation section. As the experimental results will show, the proposed method has good performance in large ULA.

4. Simulation results

For the highlight of the proposed method is to exploit the property of mixed non-circular sources, it is supposed to compare its performance with other methods dealing with mixed non-circular sources. However, to the best of my knowledge, the existing methods are aimed at either pure non-circular sources or mixed circular sources. Thus, we divide the performance analyses into three parts: the performance analyses for mixed non-circular sources, the performance analyses for pure far-field non-circular sources and the performance analyses for pure near-field non-circular sources.

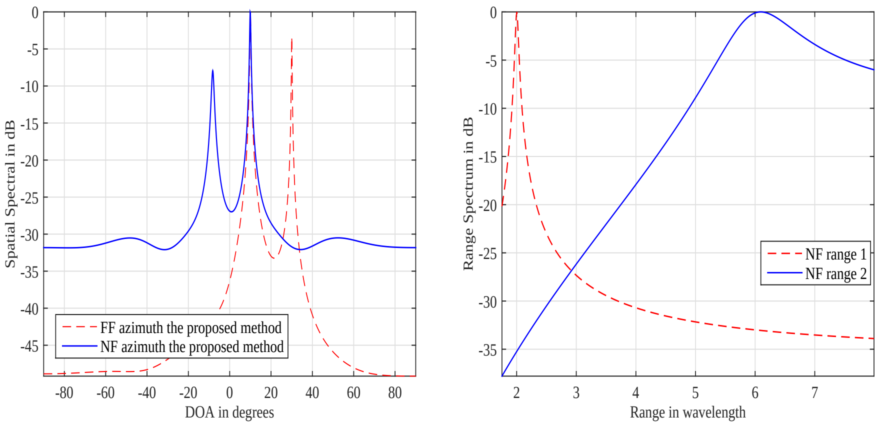

(a) (b)

(a). Spatial spectrum for azimuth estimations.

(b). Spatial spectrum for range estimations.

Fig. 2: Spatial spectrum for the DOA and range estimation results of mixed non-circular sources: $\theta_1 = -8°$, $r_1 = 2\lambda$, $\theta_2 = 10°$, $r_2 = 6\lambda$, $\theta_3 = 10°$, $r_3 = +\infty$, $\theta_4 = 30°$, $r_4 = +\infty$, SNR = 15 dB, and the number of snapshots is 500.

For all simulations in this section, the inter-sensor spacing of a ULA is quarter-wavelength ($d = \lambda/4$) and the impinging sources are BPSK signals with the additive noise being spatially and temporally white complex Gaussian. The root mean square error (RMSE) is adopted as a performance metric.

In subsection 1 to subsection 3, a ULA of 9 sensors ($L = 4$) is employed, and its Fresnel region is $1.75\lambda < r < 8\lambda$.

4.1. Mixed non-circular sources

In this subsection, we examine the DOAs and ranges of the proposed method compared with that of some other methods under the mixed far-field and near-field non-circular sources.

4.1.1. DOAs estimation

The scenario of two near-field and two far-field non-circular sources impinging on the ULA is assumed. They are located at $(-8°, 2\lambda)$, $(10°, 6\lambda)$ and

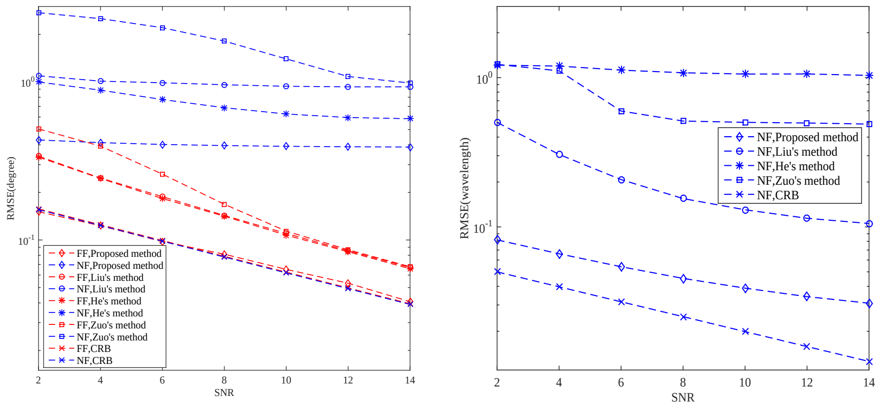

(a)

(b)

(a). RMSEs for DOA estimation versus SNR.

(b). RMSEs for range estimation versus SNR.

Fig. 3: RMSEs for DOA and range estimation for mixed non-circular sources versus SNR: $\theta_1 = 5°$, $r_1 = 1.9\lambda$, $\theta_2 = 30°$, $r_2 = 2.6\lambda$, $\theta_3 = -25°$, $r_3 = +\infty$, $\theta_4 = 5°$, $r_4 = +\infty$, and the number of snapshots is 500 with 500 independent trials.

$(10°, +\infty)$, $(30°, +\infty)$, respectively. The SNR is 15 dB and the number of snapshots is 500. The resultant spatial spectrum for DOA and range estimation are shown in Fig. 2. Clearly both the DOAs and relevant ranges have been identified successfully. Besides, the proposed algorithm is applicable to the scenario that the near-field sources and the far-field sources have the same azimuth.

4.1.2. Performance versus SNR

Consider two near-field signals located at $(5°, 1.9\lambda)$, $(30°, 2.6\lambda)$ and two far-field signals located at $(-25°, +\infty)$, $(5°, +\infty)$, respectively. Fig. 3 shows the RMSE results of the azimuth and range estimations after 500 independent trials. The SNR varies from 2 dB to 14 dB with the number of snapshots fixed at 500. Besides, the results obtained by He's method [23], Zuo's method [26] and Liu's method [27] all of which are designed for mixed circular sources, are also provided for comparisons in this figure. In addition, the deterministic CRB is also shown as a benchmark [32]. From the results, we can see that the proposed

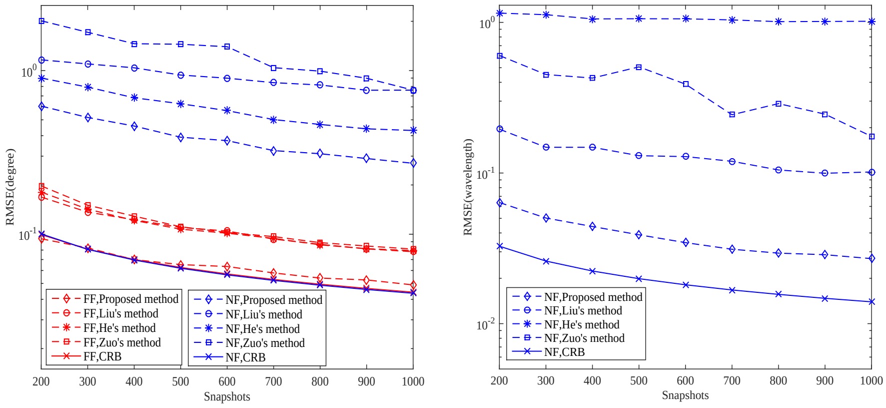

(a)

(b)

(a). RMSEs for DOA estimation versus snapshots.

(b). RMSEs for range estimation versus snapshots.

Fig. 4: RMSEs for DOA and range estimation for mixed non-circular sources versus snapshots: $\theta_1 = 5°$, $r_1 = 1.9\lambda$, $\theta_2 = 30°$, $r_2 = 2.6\lambda$, $\theta_3 = -25°$, $r_3 = +\infty$, $\theta_4 = 5°$, $r_4 = +\infty$, and SNR = 10dB with 500 independent trials.

algorithm consistently outperforms the other three algorithms in both azimuth and range estimations.

4.1.3. Performance versus snapshots

The incident signals are the same as the second set of simulations in this subsection. The number of snapshots varies from 200 to 1000, with the SNR fixed at 10dB. In addition, three methods in the second set of simulations and the criterion for evaluation provided in [32] are also presented for comparisons in Fig. 4. From the results, we can see that the proposed method has achieved the best performance over the considered region again.

From the simulations above, we note that the methods in [23, 26, 27] which are transplanted to deal with mixed non-circular sources have worse performances than the proposed methods derived for mixed non-circular sources. To this degree, it exactly proves the significance to exploit the characteristic of non-circular sources. In addition, the reasonable design of the proposed method

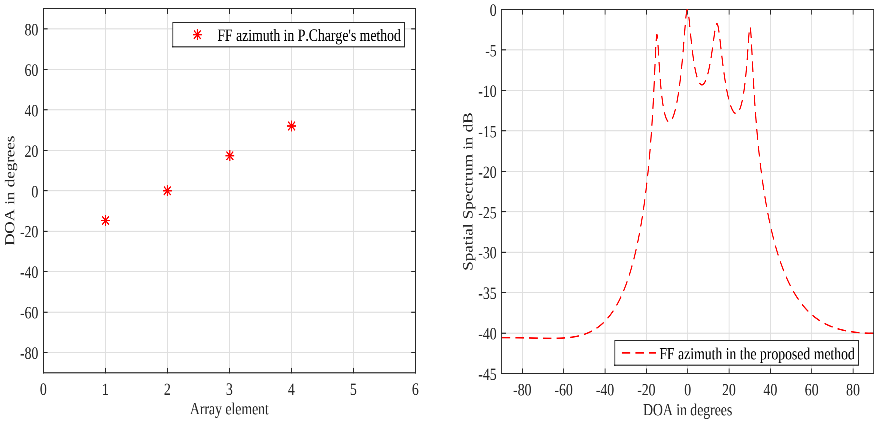

(a) (b)

(a). Azimuth estimations with the method in [11].

(b). Azimuth estimations with the proposed method.

Fig. 5: DOA estimation results of pure far-field non-circular sources: $\theta_1 = -15°$, $r_1 = +\infty$, $\theta_2 = 0°$, $r_2 = +\infty$, $\theta_3 = 15°$, $r_3 = +\infty$, $\theta_4 = 30°$, $r_4 = +\infty$, SNR = 10 dB, and the number of snapshots is 500.

is another factor contributing to the performance as shown in the following simulations.

4.2. Pure far-field non-circular sources

In this subsection, the DOA estimation of the proposed method with the pure far-field non-circular sources which is considered as a special case of the mixed non-circular sources is performed. And as P.Charge's method in[11] explores the nature of pure far-field non-circular sources with polynomial rooting technique, it is added as a comparison in the following simulations.

4.2.1. DOAs estimation

The azimuth estimation for pure far-field non-circular sources are performed based on the method in [11] and the proposed method, respectively. Four far-field non-circular sources located at $(-15°, +\infty)$, $(0°, +\infty)$, $(15°, +\infty)$ and $(30°, +\infty)$ impinging on the ULA are considered. The SNR is 10 dB and the

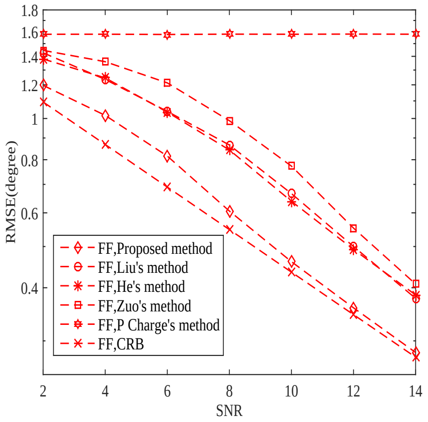

Fig. 6: RMSEs for DOA estimation of pure far-field non-circular sources versus SNR: $\theta_1 = -15°$, $r_1 = +\infty$, $\theta_2 = 0°$, $r_2 = +\infty$, $\theta_3 = 15°$, $r_3 = +\infty$, $\theta_4 = 30°$, $r_4 = +\infty$, and the number of snapshots is 500 with 500 independent trials.

number of snapshots is 500. In Fig. 5, it's proved that both these two methods can estimate the DOAs of pure far-field non-circular sources successfully. However, it has to be pointed out that when the DOA separations among the sources become closer, the performance of the method in [11] will deteriorate rapidly (not shown in the figure).

4.2.2. Performance versus SNR

The impinging signals are the same as the first set of experiments in this subsection. The SNR ranges from 2 dB to 14 dB with the number of snapshots fixed at 500. Together with the result in [11], the results from the methods in [23, 26, 27, 32] for pure far-field non-circular sources are also plotted in Fig. 6. It's apparent that even though [11] is designed for pure far-field non-circular sources, its performance is unsatisfactory. For those methods aimed at mixed circular sources, they have lower accuracy than the proposed method specially derived for mixed non-circular sources.

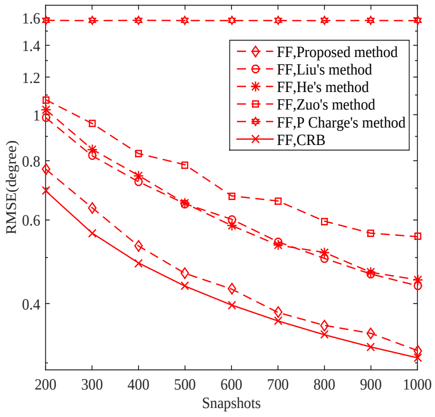

Fig. 7: RMSEs for DOA estimation of pure far-field non-circular sources versus snapshot: $\theta_1 = -15^\circ$, $r_1 = +\infty$, $\theta_2 = 0^\circ$, $r_2 = +\infty$, $\theta_3 = 15^\circ$, $r_3 = +\infty$, $\theta_4 = 30^\circ$, $r_4 = +\infty$, SNR = 10dB with 500 independent trials.

4.2.3. Performance versus snapshots

The simulation conditions are similar to those in the second example in this subsection, except that the number of snapshots varies from 200 to 1000, with the SNR set at 10dB. The results of the performance can be obtained from Fig. 7, and the proposed method shows the best capability among these methods.

4.3. Pure near-field noncircular sources

In this subsection, the azimuth and range estimations for the proposed method under the pure near-field non-circular sources which is treated as another special case of the mixed non-circular sources is conducted. And the method in [20] which is aimed at the pure near-field non-circular sources is supplemented to the simulations.

4.3.1. DOAs Estimation

Let's consider the scenario of four near-field non-circular sources impinging on the ULA. They are located at $(-10^\circ, 1.8\lambda)$, $(0^\circ, 2\lambda)$, $(20^\circ, 2.2\lambda)$ and $(30^\circ, 2.4\lambda)$, respectively. The SNR is 15 dB and the number of snapshots is 500. In Fig. 8, it's clear that the DOAs estimation of Xie's method brings some

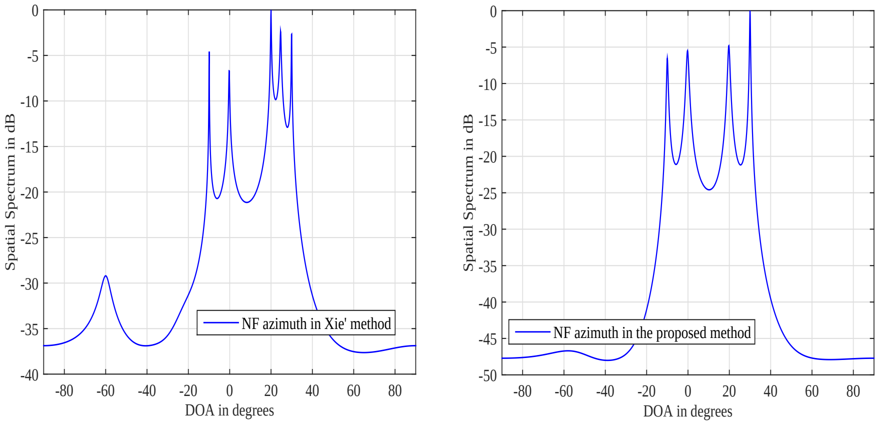

(a) (b)

(a). Azimuth estimations with the method in [20].

(b). Azimuth estimations with the proposed method.

Fig. 8: Spatial spectrum for the DOA estimation results of pure near-field non-circular sources: $\theta_1 = -10^\circ$, $r_1 = 1.8\lambda$, $\theta_2 = 0^\circ$, $r_2 = 2\lambda$, $\theta_3 = 20^\circ$, $r_3 = 2.2\lambda$, $\theta_4 = 30^\circ$, $r_4 = 2.4\lambda$, SNR = 15 dB, and the number of snapshots is 500.

pseudo-peaks while the proposed method doesn't. In Xie's simulation results, we remove the pseudo-peaks and use the reliable estimation value of DOAs to get the range of near-field sources (for the following simulations in *Performance versus SNR* and *Performance versus snapshots* of this subsection, the same preprocessing is conducted for Xie's method). The related spatial spectrum for range estimation by Xie's method is shown in Fig. 9(a). And the proposed method's related spatial spectrum for range estimation is shown in Fig. 9(b). Through Fig. 9, we can see that two of them can identify the ranges successfully.

4.3.2. Performance versus SNR

In this part, the performance comparison for the proposed method versus SNR is performed. The parameter settings are the same with the *DOAs estimation* in this subsection except for the SNR varying from 2dB to 14dB. The

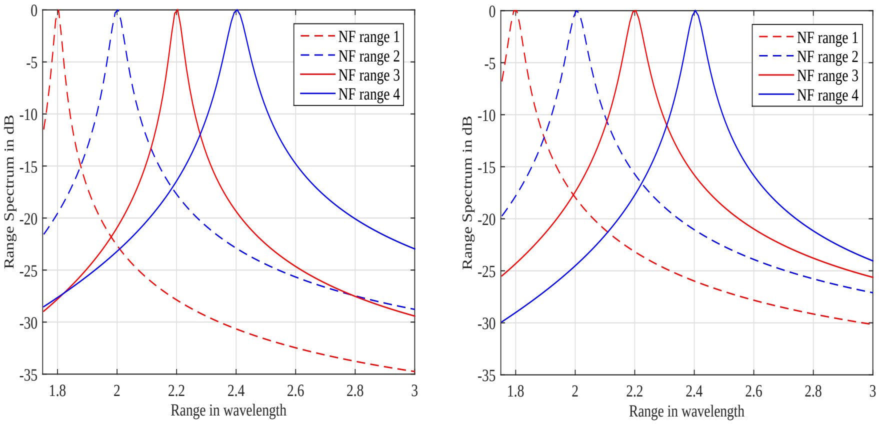

(a)

(b)

(a). Range estimations with the method in [20].

(b). Range estimations with the proposed method.

Fig. 9: The range estimation results of pure near-field non-circular sources: $\theta_1 = -10°$, $r_1 = 1.8\lambda$, $\theta_2 = 0°$, $r_2 = 2\lambda$, $\theta_3 = 20°$, $r_3 = 2.2\lambda$, $\theta_4 = 30°$, $r_4 = 2.4\lambda$, SNR = 15 dB, and the number of snapshots is 500.

corresponding experiments of the methods in [23, 26, 27, 32] are also performed. From Fig. 10, we can see that the performance of the proposed method exceeds Xie's method by a narrow margin. This is because Xie's selection matrices $\mathbf{J}_1$ and $\mathbf{J}_2$ (see Lemma 1, [20]) determine that only part of the extended near-field steering matrix can be utilized to examine the DOAs of near-field sources, while the proposed method takes the whole extended near-field steering matrix into consideration (formulation (26) in 11th page).

4.3.3. Performance versus snapshots

In this set of simulations, we assess the performance of the proposed method versus the number of snapshots. The incident signals and simulation conditions are the same as *DOAs estimation* in this subsection. The number of snapshots is between 200 and 1000 with SNR fixed at 10dB. Fig. 11 shows the RMSE results of the azimuth and range estimations, where we can see that the proposed

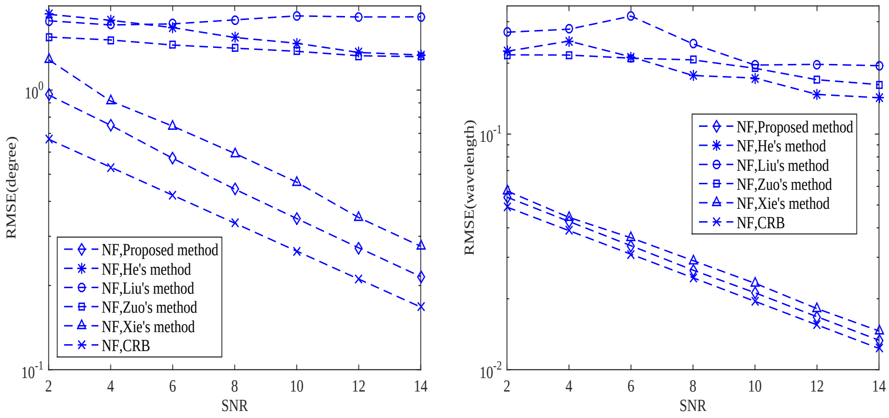

(a)

(b)

(a). RMSEs for DOA estimation versus SNR.

(b). RMSEs for Range estimation versus SNR.

Fig. 10: RMSEs for DOA and range estimation for pure near-field non-circular sources versus SNR: $\theta_1 = -10°$, $r_1 = 1.8\lambda$, $\theta_2 = 0°$, $r_2 = 2\lambda$, $\theta_3 = 20°$, $r_3 = 2.2\lambda$, $\theta_4 = 30°$, $r_4 = 2.4\lambda$, and the number of snapshots fixed at 500, with 500 independent trials.

algorithm has a better performance.

The experiments in subsection *4.2* and subsection *4.3* explore two special cases of mixed non-circular sources, respectively. As the simulation results have shown, the proposed method outperforms other methods designed for circular sources or pure non-circular sources. Therefore, these experiments are convincing proofs that the proposed method is an effective localization method for non-circular sources.

4.4. Array aperture verification

For all simulations in this subsection, a ULA of 7 sensors (L= 3) is assumed, and its Fresnel region is $1.14\lambda < r < 4.5\lambda$. The SNR is fixed at 15 dB and the number of snapshots is 200.

In the first simulation, as a most general case, four far-field non-circular sources (they are located at $(0°, +\infty)$, $(20°, +\infty)$, $(30°, +\infty)$ and $(50°, +\infty)$, respectively) and two near-field non-circular sources (they are located at $(-20°, 1.5\lambda)$

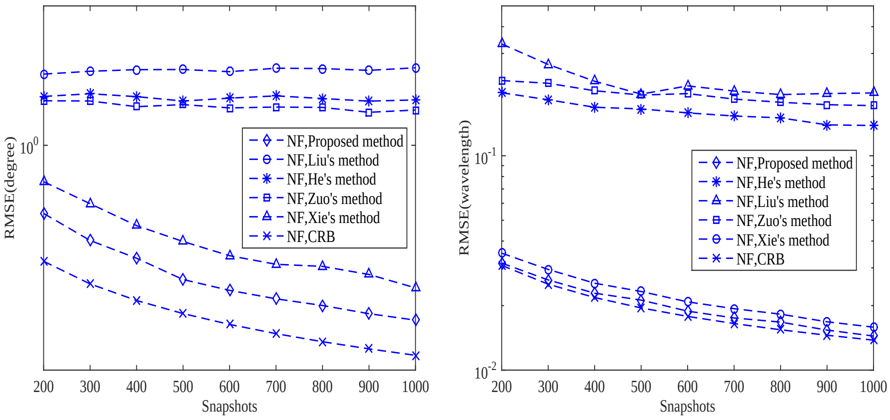

(a) (b)

(a). RMSEs for DOA estimation versus snapshots.

(b). RMSEs for Range estimation versus snapshots.

Fig. 11: RMSEs for DOA and range estimation for pure near-field non-circular sources versus the number of snapshots: $\theta_1 = -10°$, $r_1 = 1.8\lambda$, $\theta_2 = 0°$, $r_2 = 2\lambda$, $\theta_3 = 20°$, $r_3 = 2.2\lambda$, $\theta_4 = 30°$, $r_4 = 2.4\lambda$, and the SNR fixed at 10dB, with 500 independent trials.

and $(0°, 2\lambda)$, respectively) coexist. Fig. 12(a) shows the DOA estimation results of these six impinging sources, and Fig. 12(b) demonstrates the range estimation results of these two near-field sources. Apparently, both the DOAs and relevant ranges have been identified correctly.

In the second one, six far-field non-circular sources are assumed to imping on the ULA. They are located at $(-40°, +\infty)$, $(-20°, +\infty)$, $(0°, +\infty)$, $(20°, +\infty)$, $(40°, +\infty)$ and $(60°, +\infty)$, respectively. As Fig. 13 (at the top of 27th page) shows, all the estimated DOAs of the far-field sources are consistent with the original DOAs.

In the last case, there are six near-field non-circular sources located at $(-40°, 1.2\lambda)$, $(-20°, 1.3\lambda)$, $(0°, 1.4\lambda)$, $(20°, 1.5\lambda)$, $(40°, 1.6\lambda)$, and $(60°, 2\lambda)$, respectively. The resultant spatial spectrum for DOA and range estimation is shown in Fig. 14 (at the top of 28th page). Clearly the proposed method have accurately estimated the DOAs and relevant ranges.

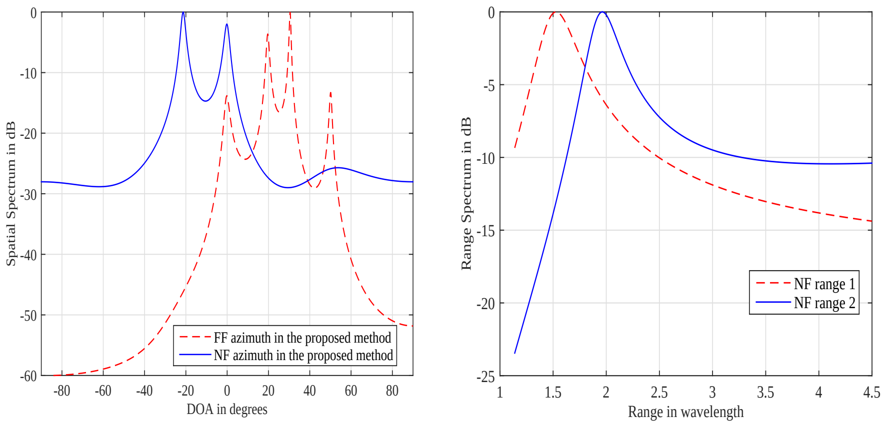

(a) (b)

(a). Azimuth estimations. (b). Range estimation.

Fig. 12: Array aperture's verification test for the DOA and range estimation results of mixed non-circular sources: $\theta_1 = 0°$, $r_1 = +\infty$, $\theta_2 = 20°$, $r_2 = +\infty$, $\theta_3 = 30°$, $r_3 = +\infty$,$\theta_4 = 50°$, $r_4 = +\infty$, $\theta_5 = -20°$, $r_5 = 1.5\lambda$, $\theta_6 = 0°$, $r_6 = 2\lambda$, SNR $=$ 15 dB, and the number of snapshots is 200.

From the simulation results in this subsection, we verify that the maximum number of sources which can be distinguished by the proposed method is $2L$ with a ULA composed of $2L+1$ sensors.

4.5. Suitability test for massive MIMO system

To show the suitability of the proposed method for the massive MIMO system, the performance test versus the number of array element is carried out in this subsection. Suppose there are two far-field strictly non-circular sources impinging upon a large ULA consisting of M elements at directions $\theta_1 = -12.1°, \theta_2 = 15°$. The SNR and the number of snapshots are fixed at 0dB and 200, respectively. Again, the methods in [23, 26, 27] are adopted as comparisons. As Fig. 15 (at the top of 29th page) shows, the RMSEs of all algorithms decrease monotonously when the number of elements increases, which means that these algorithms are suitable for massive MIMO scenarios.

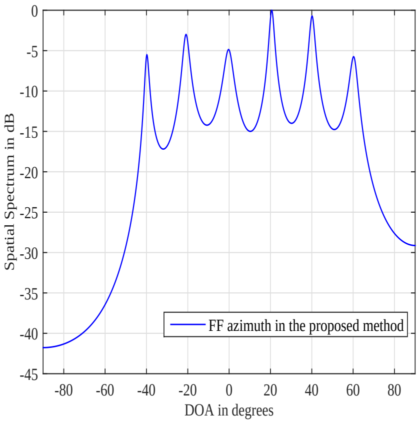

Fig. 13: Array aperture's verification test for the DOA estimation results of pure far-field non-circular sources: $\theta_1 = -40°$, $r_1 = +\infty$, $\theta_2 = -20°$, $r_2 = +\infty$, $\theta_3 = 0°$, $r_3 = +\infty$, $\theta_4 = 20°$, $r_4 = +\infty$, $\theta_5 = 40°$, $r_5 = +\infty$, $\theta_6 = 60°$, $r_6 = +\infty$, SNR = 15 dB, and the number of snapshots is 200.

5. Conclusion

In this paper, an effective localization method for a mixture of near-field and far-field non-circular sources has been proposed based on a large centrosymmetric ULA. The proposed method makes full use of the property of the impinging sources and the tricks of the traditional source localization methods, where the extended received data model is constructed by utilizing the non-circularity of the incident sources and the DOA and range estimation problems are separated into three 1-dimensional parameter estimation problems solved by the conventional MUSIC algorithm and the generalized ESPRIT method, respectively. As verified by the simulation results, the proposed method has achieved a better DOA and range estimation performance than all the considered existing methods. In addition, the proposed method is suitable for massive MIMO system.

Acknowledgement

This work was supported by the Civil Aerospace Foundation, and the National Natural Science Foundation of China under Grant No. 61871282 and

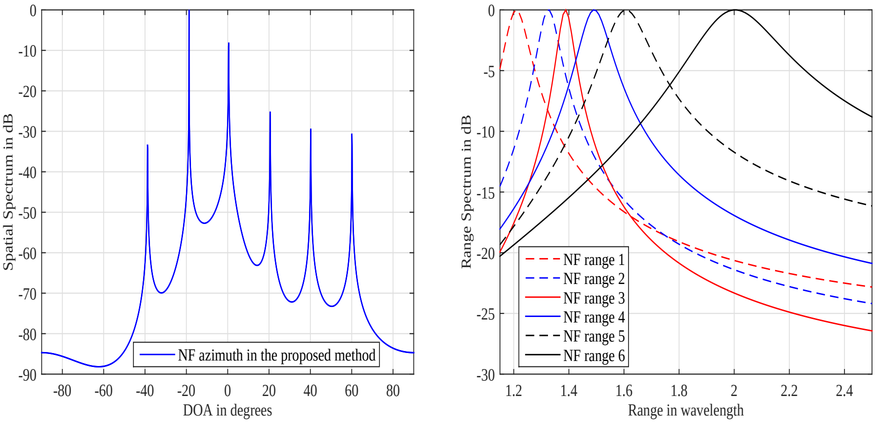

(a)

(b)

(a). Azimuth estimations.

(b). Range estimation.

Fig. 14: Array aperture's verification test for the DOA and range estimation results of pure near-field non-circular sources: $\theta_1 = -40°$, $r_1 = 1.2\lambda$, $\theta_2 = -20°$, $r_2 = 1.3\lambda$, $\theta_3 = 0°$, $r_3 = 1.4\lambda$, $\theta_4 = 20°$, $r_4 = 1.5\lambda$, $\theta_5 = 40°$, $r_5 = 1.6\lambda$, $\theta_6 = 60°$, $r_6 = 2\lambda$, SNR = 15 dB, and the number of snapshots is 200.

61601261, and by Zhejiang Provincial Natural Science Foundation of China under Grant LQ19F010002, and by Natural Science Foundation of Ningbo Municipality under Grant No. 2018A610094.

References

[1] E. Bjornson, L. Sanguinetti, H. Wymeersch, J. Hoydis, T. L. Marzetta, Massive MIMO is a reality - what is next? five promising research directions for antenna arrays, submitted to Digital Signal Processing. [Online]. Available: https://arxiv.org/abs/1902.07678v1.

[2] E. G. Larsson, O. Edfors, F. Tufvesson, T. L. Marzetta, Massive MIMO for next generation wireless systems, IEEE Communications Magazine 52 (2) (2014) 186–195. doi:10.1109/MCOM.2014.6736761.

[3] H. Yin, D. Gesbert, M. Filippou, Y. Liu, A coordinated approach

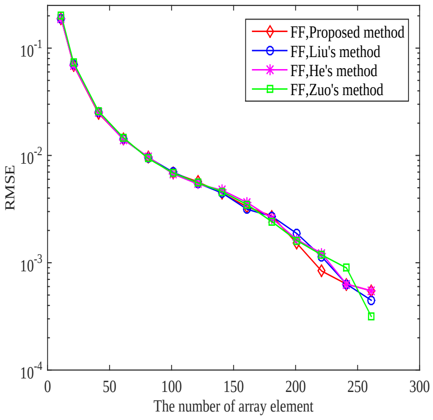

Fig. 15: RMSE versus the number of array element: $\theta_1 = -12.1°$, $\theta_2 = 0°$, SNR $= 0$ dB, and the number of snapshots is 200 with 500 independent trials.

to channel estimation in large-scale multiple-antenna systems, IEEE Journal on Selected Areas in Communications 31 (2) (2013) 264–273. doi:10.1109/JSAC.2013.130214.

[4] S. He, Y. Huang, H. Wang, S. Jin, L. Yang, Leakage-aware energy-efficient beamforming for heterogeneous multicell multiuser systems, IEEE Journal on Selected Areas in Communications 32 (6) (2014) 1268–1281. doi:10.1109/JSAC.2014.2328142.

[5] J. Jose, A. Ashikhmin, T. L. Marzetta, S. Vishwanath, Pilot contamination and precoding in multi-cell TDD systems, IEEE Transactions on Wireless Communications 10 (8) (2011) 2640–2651. doi:10.1109/TWC.2011.060711.101155.

[6] A. Hu, T. Lv, H. Gao, Y. Lu, E. Liu, Pilot design for large-scale multi-cell multiuser MIMO systems, in: 2013 IEEE International Conference on Communications (ICC), 2013, pp. 5381–5385. doi:10.1109/ICC.2013.6655444.

[7] O. N. Alrabadi, E. Tsakalaki, H. Huang, G. F. Pedersen, Beamforming via large and dense antenna arrays above a clutter, IEEE

Journal on Selected Areas in Communications 31 (2) (2013) 314–325. doi:10.1109/JSAC.2013.130218.

[8] Z. Shi, C. Zhou, Y. Gu, N. A. Goodman, F. Qu, Source estimation using coprime array: A sparse reconstruction perspective, IEEE Sensors Journal 17 (3) (2017) 755–765. doi:10.1109/JSEN.2016.2637059.

[9] C. Zhou, Y. Gu, Y. D. Zhang, Z. Shi, T. Jin, X. Wu, Compressive sensing-based coprime array direction-of-arrival estimation, IET Communications 11 (11) (2017) 1719–1724. doi:10.1049/iet-com.2016.1048.

[10] F. Gao, A. B. Gershman, A generalized ESPRIT approach to direction-of-arrival estimation, IEEE Signal Processing Letters 12 (3) (2005) 254–257. doi:10.1109/LSP.2004.842276.

[11] P. Charge, Y. Wang, J. Saillard, A non-circular sources direction finding method using polynomial rooting, Signal Processing 81 (8) (2001) 1765 – 1770, special section on Signal Processing Techniques for Emerging Comm unications Applications. doi:10.1016/S0165-1684(01)00071-8.

[12] C. Zhou, Y. Gu, X. Fan, Z. Shi, G. Mao, Y. D. Zhang, Direction-of-arrival estimation for coprime array via virtual array interpolation, IEEE Transactions on Signal Processing 66 (22) (2018) 5956–5971. doi:10.1109/TSP.2018.2872012.

[13] C. Zhou, Y. Gu, S. He, Z. Shi, A robust and efficient algorithm for coprime array adaptive beamforming, IEEE Transactions on Vehicular Technology 67 (2) (2018) 1099–1112. doi:10.1109/TVT.2017.2704610.

[14] C. Zhou, Y. Gu, Z. Shi, Y. D. Zhang, Off-grid direction-of-arrival estimation using coprime array interpolation, IEEE Signal Processing Letters 25 (11) (2018) 1710–1714. doi:10.1109/LSP.2018.2872400.

[15] C. Zhou, Z.Shi, Y. Gu, X. Shen, DECOM: DOA estimation with combined MUSIC for coprime array, in: 2013 International Confer-

ence on Wireless Communications and Signal Processing, 2013, pp. 1–5. doi:10.1109/WCSP.2013.6677080.

[16] F. Wen, Computationally efficient DOA estimation algorithm for MIMO radar with imperfect waveforms, IEEE Communications Letters 23 (6) (2019) 1037–1040. doi:10.1109/LCOMM.2019.2911285.

[17] Y. Wu, H. C. So, C. Hou, J. Li, Passive localization of near-field sources with a polarization sensitive array, IEEE Transactions on Antennas and Propagation 55 (8) (2007) 2402–2408. doi:10.1109/TAP.2007.901912.

[18] E. Grosicki, K. Abed-Meraim, Y. Hua, A weighted linear prediction method for near-field source localization, IEEE Transactions on Signal Processing 53 (10) (2005) 3651–3660. doi:10.1109/TSP.2005.855100.

[19] W. Zhi, M. Y. Chia, Near-field source localization via symmetric subarrays, IEEE Signal Processing Letters 14 (6) (2007) 409–412. doi:10.1109/LSP.2006.888390.

[20] J. Xie, H. Tao, X. Rao, J. Su, Efficient method of passive localization for near-field noncircular sources, IEEE Antennas and Wireless Propagation Letters 14 (2015) 1223–1226. doi:10.1109/LAWP.2015.2399534.

[21] S. Payami, F. Tufvesson, Channel measurements and analysis for very large array systems at 2.6 GHz, in: 2012 6th European Conference on Antennas and Propagation (EUCAP), 2012, pp. 433–437. doi:10.1109/EuCAP.2012.6206345.

[22] J. Liang, D. Liu, Passive localization of mixed near-field and far-field sources using two-stage MUSIC algorithm, IEEE Transactions on Signal Processing 58 (1) (2010) 108–120. doi:10.1109/TSP.2009.2029723.

[23] J. He, M. N. S. Swamy, M. O. Ahmad, Efficient application of MUSIC algorithm under the coexistence of far-field and near-field sources, IEEE Transactions on Signal Processing 60 (4) (2012) 2066–2070. doi:10.1109/TSP.2011.2180902.

[24] J. Jiang, F. Duan, X. Wang, An efficient classification method of mixed sources, IEEE Sensors Journal 16 (10) (2016) 3731–3734. doi:10.1109/JSEN.2016.2533622.

[25] J. Jiang, F. Duan, J. Chen, Y. Li, X. Hua, Mixed near-field and far-field sources localization using the uniform linear sensor array, IEEE Sensors Journal 13 (8) (2013) 3136–3143. doi:10.1109/JSEN.2013.2257735.

[26] W. Zuo, J. Xin, J. Wang, N. Zheng, A. Sano, A computationally efficient source localization method for a mixture of near-field and far-field narrowband signals, in: 2014 IEEE International Conference on A-coustics, Speech and Signal Processing (ICASSP), 2014, pp. 2257–2261. doi:10.1109/ICASSP.2014.6854001.

[27] G. Liu, X. Sun, Efficient method of passive localization for mixed far-field and near-field sources, IEEE Antennas and Wireless Propagation Letters 12 (2013) 902–905. doi:10.1109/LAWP.2013.2273451.

[28] H. Chen, C. Hou, W. Zhu, W. Liu, Y. Dong, Z. Peng, Q. Wang, ESPRIT-like two-dimensional direction finding for mixed circular and strictly noncircular sources based on joint diagonalization, Signal Processing 141 (2017) 48 – 56. doi:10.1016/j.sigpro.2017.05.024.

[29] H. Chen, C. Hou, W. Liu, W. Zhu, M. N. S. Swamy, Efficient two-dimensional direction-of-arrival estimation for a mixture of circular and noncircular sources, IEEE Sensors Journal 16 (8) (2016) 2527–2536. doi:10.1109/JSEN.2016.2517128.

[30] H. Chen, W. Wang, W. Liu, Joint DOA, range, and polarization estimation for rectilinear sources with a COLD array, IEEE Wireless Communications Letters (2019) 1–1doi:10.1109/LWC.2019.2919542.

[31] J. Xin, N. Zheng, A. Sano, Simple and efficient nonparametric method for estimating the number of signals without eigendecomposi-

tion, IEEE Transactions on Signal Processing 55 (4) (2007) 1405–1420. doi:10.1109/TSP.2006.889982.

[32] H. Chen, W. Zhu, W. Liu, M. Swamy, Y. Li, Q. Wang, Z. Peng, RARE-based localization for mixed near-field and far-field rectilinear sources, Digital Signal Processing 85. doi:10.1016/j.dsp.2018.11.006.

[33] J. Liu, Z. Huang, Y. Zhou, Extended 2q-MUSIC algorithm for noncircular signals, Signal Processing 88 (6) (2008) 1327–1339. doi:10.1016/j.sigpro.2007.11.012.

[34] H. Krim, M. Viberg, Two decades of array signal processing research: the parametric approach, IEEE Signal Processing Magazine 13 (4) (1996) 67–94. doi:10.1109/79.526899.

[35] B. D. Rao, K. V. S. Hari, Weighted subspace methods and spatial smoothing: analysis and comparison, IEEE Transactions on Signal Processing 41 (2) (1993) 788–803. doi:10.1109/78.193218.

Qing Wang received the B.Eng., M.Eng., and Ph.D. degrees in electronic engineering from Tianjin University, Tianjin, China, in 2004, 2007, and 2010, respectively. Since 2010, she has been with the School of Electronic and Information Engineering, Tianjin University, where she is currently an Associate Professor. From 2007 to 2009, she was a Visiting Student with the School of Electrical and Electronic Engineering, Nanyang Technological University, Singapore. From 2018 to 2019, she is a Visiting Scholar at Columbia University in the City of New York, USA. Her research interests include wireless communication, passive radar, signal processing in the general area of communication and networkand intelligent signal processing.

Xian Wang was born in Hubei, China, on May 5, 1995. She received the B.Sc degree in communication engineering from Hainan University of China in 2017, and she is currently pursuing M.Sc degree in information and communication engineering with the School of Electrical and Information Engineering at Tianjin University under the guidance of associate professor Qing Wang. Her research interest is array signal processing.

Hua Chen received the M.Eng. degree and Ph.D. degree in Information and Communication Engineering from Tianjin University, Tianjin, China, in 2013 and 2017, respectively. He is now as a lecturer in Faculty of Information Science and Engineering, Ningbo University, China. His research interests include array signal processing, MIMO radar and passive radar.

Xiaotian Zhu received the B.Sc degree in electronic information engineering from Changchun University of Science and Technology, China. He received M.Sc degree in electromagnetic field and microwave technology from Tianjin University, China. And his research interests include array signal processing and passive MIMO.

Wei Liu received his B.Sc. in Space Physics (minor in Electronics) in 1996, L.L.B. in Intellectual Property Law in 1997, both from Peking University, China, M.Phil. from the Department of Electrical and Electronic Engineering, University of Hong Kong, in 2001, and Ph.D. in 2003 from the Communications Research Group, School of Electronics and Computer Science, University of Southampton, UK. He then worked as a postdoc in the same group and later in the Communications and Signal Processing Group, Department of Electrical and Electronic Engineering, Imperial College London. Since September 2005, he has been with the Communications Research Group, Department of Electronic and Electrical Engineering, University of Sheffield, UK, as a lecturer, and then a senior lecturer. His research interests are mainly in sensor array signal processing, blind signal processing, multirate signal processing and their various applications in wireless communications, sonar, radar, satellite navigation, speech enhancement and biomedical engineering.

Weiqing Yan received the Ph.D. degree in the School of Electronic Information Engineering, Tianjin University, Tianjin, China, in 2017. She was a Visiting Student with University of California at Berkeley, Berkeley, CA, USA, from 2015 to 2016. She is currently a faculty Member with the School of Computer and Control Engineering, Yantai University, Yantai, China. Her research interests include 3D image editing, computer graphic, computer vision and array signal processing.

Laihua Wang received the B.S. degree in electronic engineering from Yantai University, Yantai, China, in 2010. She received the Ph.D. degree in the School of Electronic Information Engineering, Tianjin University, Tianjin, China, in 2016. She is currently a faculty Member with School of software, Qufu Normal University, China, Jining, China. Her research interests include virtual view image synthesis, multiview video coding and array signal processing.